Title

Nanoscale integration of oxides and metals in bulk 3D composites: leveraging SrFe12O19/Co interfaces for magnetic exchange coupling

Journal

Journal of Materials Science, 54(11)

ISSN

0022-2461

Authors

Volodchenkov, AD
Kodera, Y
Garay, JE

Publication Date

2019-06-01

DOI

10.1007/s10853-019-03323-z

Peer reviewed

J Mater Sci (2019) 54:8276–8288

Composites

Nanoscale integration of oxides and metals in bulk 3D composites: leveraging $SrFe_{12}O_{19}$/Co interfaces for magnetic exchange coupling

A. D. Volodchenkov[1], Y. Kodera[1,2,*], and J. E. Garay[1,2,*]

[1] *Advanced Materials Processing and Synthesis (AMPS) Laboratory, University of California, San Diego, CA, USA*
[2] *Materials Science and Engineering Program, Mechanical and Aerospace Engineering Department, University of California, San Diego, CA, USA*

Received: 11 September 2018
Accepted: 3 January 2019
Published online: 15 February 2019

ABSTRACT

The integration of different material classes (e.g, oxides and metals) with nanoscale dimensions in large 3D materials remains a fundamental challenge in nanocomposite fabrication. The incentive is that some of the most interesting properties occur at nanoscale interfaces, while the challenge arises from the difficulty in densifying the materials without deleterious reaction at the interface. Here, we introduce a method based on the synthesis of core–shell powders followed by efficient, relatively low-temperature densification with current-activated pressure-assisted densification. The composition of the bulk nanocomposites can be controlled by varying the core–shell weight ratio, leading to controllable thicknesses of the hard/soft magnetic phases. We demonstrate intimate mixtures of nanoscale strontium ferrite (hard magnetic phase) and Co–Fe (soft magnetic phase) with minimal reaction. The high volume content of high-quality oxide/metal interfaces leads to magnetic exchange coupling in the composites.

Introduction and background

The integration of dissimilar phases has been the subject of intense research propelled by the unique and exciting properties that are generated at the interface between nanoscale phases in intimate contact [1]. Successes in fabricating thin film oxide/metal structures have led to breakthrough advances in the study in magnetic materials, for example, giant magnetoresistance (GMR) for memory devices [2], the anomalous Hall effect in thin film nanostructures for spintronic studies [3] and exchange spring behavior for improving permanent magnets PMs [4]. Excellent grain size control and intimate mixing of oxide/metal phases leading to exchange coupling have also been demonstrated in nanopowders [5–7]. The exchange spring concept [8] requires a high volume concentration of high-quality interfaces between hard and soft magnetic phases and is a

Address correspondence to E-mail: ykodera@ucsd.edu; jegaray@ucsd.edu

https://doi.org/10.1007/s10853-019-03323-z

promising way of reducing the rare earth content in permanent magnets.

Despite these advances, the integration of well-mixed nanoscale oxide and metal phases has proven more elusive in bulk samples (with millimeter to centimeter dimensions). Fabrication of bulk nanomaterials by densifying core–shell nanopowders is a natural approach to achieve nanoscale mixing and high-quality interfaces, since the mixing is 'built in' at the powder level. As shown schematically in Fig. 1, oxide 'core' particles can be covered with a metal 'shell' to form a core–shell powder. If the core shell composite powder can be properly densified, it should be possible to retain the nanoscale mixing imparted by the original powder structure. The fundamental challenge is *achieving densification* (pore removal) of oxide/metal composite, while *minimizing reaction* between the oxide and metal phases which would cause degradation of the nanostructure by the unwanted reaction. The difficulty of course arises because the densification process requires elevated temperature which naturally increases reaction kinetics.

Here, we report a successful method based on the densification of core/shell powders to achieve dense oxide/metal nanocomposites with centimeter dimensions. The key is optimizing the oxide/metal composite powder composition and size for densification as opposed to optimization of powder as an end product. We demonstrate the method's utility and success by showing exchange coupling leading to PMs with improved magnetic energy product, commonly referred to as $(BH)_{max}$.

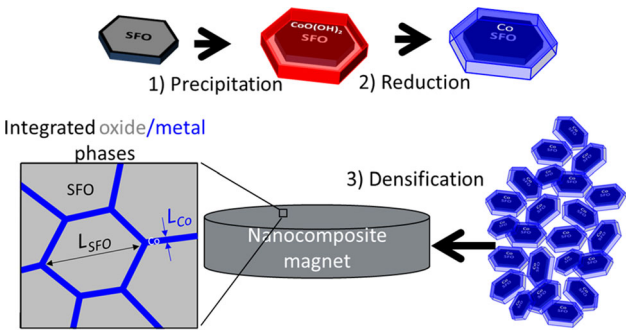

Figure 1 Roadmap to synthesis of an exchange-coupled composite based on the SFO/(Co, Fe) material system. (1) The process involves precipitation of a Co precursor, Co–O–OH, on the surface of SFO. (2) The Co precursor is then reduced to metal Co. (3) SFO/metal Co powder is densified by CAPAD into a bulk nanocrystalline exchange-coupled composite. The overall size of the materials is in the mm/cm scale, while the phases are on the hundreds of nanometers, L_{SFO} and tens of nanometers, L_{Co}.

Efficient exchange coupling in PMs (the exchange spring concept) [8] requires precise control of thickness and phase composition of a hard magnetic (in our case oxide) and soft (metal) magnetic phase. Using core shell configuration, the thickness of the soft phase can be controlled by varying the mass ratio (hard/soft) of the powder of the starting composite powder.

Our method for synthesizing composite PMs is a three-step process, shown schematically in Fig. 1. First, we use homogenous precipitation method using urea decomposition to precipitate a Co–O/Co–O-H precursor *directly on* strontium ferrite (SFO) nanoflakes, ensuring a fine degree of mixing between the hard and the soft magnetic phases. The second step is an annealing step that serves to reduce (partially convert) the soft phase precursor powder to Co/Co–O. Third, we densify the core–shell powder using current-activated pressure-assisted densification (CAPAD) [9] to achieve SFO/Co bulk nanocomposites. The result is a simple, inexpensive synthesis route for exchange-coupled bulk PM composite that *outperforms* pure SFO.

Several works have shown successfully coupled magnetic oxide-based systems using CAPAD before. Morales et al. [10] showed ferrimagnetic–antiferromagnetic coupling leading to exchange bias in iron oxide-based magnets. Zhang et al. [7] used core–shell approach to show exchange coupling in $CoFe_2O_4$/$CoFe_2$ magnetic powder composites. Zhang et al. [11] also showed successful hard/soft magnetic ferromagnetic coupling in CAPAD-densified $CoFe_2O_4$/$CoFe_2$. These previous results on utilizing the exchange spring concept yielded significantly softer magnets than the SFO/Co system presented here.

The length scales of the hard phase L_{SFO} and soft phase L_{Co} shown in Fig. 1 are critical. The ideal hard phase length scale is the single domain size which maximizes coercivity. The single domain size is ~ 500 nm [12] for SFO, so we chose a powder with close to this average particle size. For efficient exchange coupling, dimension of the soft phase should be about twice the wall thickness of magnetic domains in the hard magnetic phase (the domain wall width is a good approximation of the exchange length [13]). We can therefore approximate the exchange length as $L_{ex} \sim \pi\sqrt{A/K}$ where A is the

exchange energy constant and K is the anisotropy energy constant. Using values of $A = 3.7 \times 10^{-7}$ erg/cm (A for $BaFe_{12}O_{19}$, a very similar material used to approximate A for SFO) [14] and $K = 3.5 \times 10^6$ erg/cm^3 [15] for SFO, we find $L_{ex} = 10.5$ nm giving a total metal thickness, $L_{Co} \sim 21$ nm. The core–shell mass ratios in this work were chosen in order to achieve L_{Co} in this length range.

Our technique allows: (1) Excellent control of grain size in the nanocrystalline regime (2) ability to simultaneously densify different nanomagnetic material classes, i.e, produce large-sized intimately mixed nanocomposites (3) ability to achieve high-quality interfaces such that exchange coupling can be achieved.

Experimental procedure

Nanocomposite powder synthesis

Homogeneous precipitation is one of the most common methods of synthesizing 'monodispersed' colloids [16]. It has been used in the past to successfully synthesize a variety of different materials [17–20]. Similar to our previous work with Fe–O [6], a Co–O/Co–O–H, soft magnetic phase precursor, was synthesized through homogeneous precipitation by decomposition of urea. Co–O–H was deposited onto SFO powder ($SrFe_{12}O_{19}$, Nanostructured & Amorphous Materials Inc.). Variations of 28.7, 57.4 and 114.8 mmol of $Co(NO_3)_2$ (Sigma-Aldrich > 98%) were mixed with variations of 167, 334 and 668 mmol of $CO(NH_2)_2$, urea (Sigma-Aldrich > 99.5%) in 150 mL of H_2O. The solution was mixed with the suspension of 1.58 mmol of SFO in 50 mL of H_2O. This mixture is then heated to 90 °C and held for 1 h. To prevent further particle growth, the mixture was cooled quickly. In order to understand the effect of the amount of soft phase (Co–O) on the surface of SFO, the amount of precipitated Co–O was varied by changing the initial SFO/Co mass precipitation ratio. The SFO/Co mass precipitation ratios used were 1:1, 1:2 and 1:4 for 1 h precipitated powder. In order to understand the soft phase precipitation process, experiments were also performed without SFO (soft phase only). 57.4 mmol of $Co(NO_3)_2$ was mixed with 334 mmol of urea in 150 mL of H_2O and held at 90 °C for 2 h.

The precipitated particles were centrifuged, washed with high-purity water and centrifuged again. Decantation was used to separate powder sedimentation and liquid. The resulting powders were dried in a vacuum furnace for 24 h at 80 °C. The dried agglomerates are broken down by mortar and pestle. The powders were then reduced in a tube furnace under forming gas (5% H_2, 95% N_2) at various temperatures (250–500 °C) with 1 h ramp and no hold time at temperature. The synthesized powder was handled in inert atmosphere to prevent oxidation.

Gravimetric analysis was used to measure the yield of Co–O precipitation. The liquid collected from decantation post-precipitation was first dried on a hot plate and then calcined at 800 °C for 6 h in air to measure the amount of Co which did not precipitate. The powder post-calcination was single-phase Co_3O_4, confirmed by X-ray diffraction (XRD). The amount of collected Co_3O_4 was used to calculate precipitation yield.

For comparison, a conventionally mixed composite was also synthesized. The soft phase was homogeneously precipitated $Co(OH)_2$, reduced at 400 °C under forming gas flow, resulting in phase pure HCP Co, confirmed by XRD. SFO and Co powder were mixed using a mortar and pestle and then tumbled using conventional ball milling. This mixed with an SFO/Co mass ratio of 1:0.427 in an attempt to match the total Co amount to that of the precipitated composite powder based on the yield of the 1:2 initial SFO/Co mass precipitation ratio powder.

Powder densification (bulk nanocomposite fabrication)

Bulk samples of SFO-/Co-based composite were synthesized/densified using current-activated pressure-assisted densification CAPAD, commercially known as spark plasma sintering (SPS). The high heating and cooling rates available in CAPAD promote rapid densification allowing excellent control of grain size [9]. CAPAD has been shown to successfully densify ferrite-based magnetic materials before [10, 11, 31, 32]. We used two graphite dies similar to what has been described previously [21]. The outer die is of 38.1 mm outer diameter (OD) and 19 mm inner diameter (ID), and the inner die is of 19 mm OD and 9.56 mm ID. Graphite plungers were used for outer die and carbide plungers for inner die. A

typical experiment included a load ramp at constant voltage of 1.5 V though which the pressure was ramped from 0 to 505 MPa. Temperature typically reached 200 °C at the end of the pressure ramp. The temperature was then ramped using constant voltage ramp intervals of 0.25 V every 5 or 20 s (depending on heating rate of experiment). No hold time was used, and the system voltage was lowered to 0 V as soon as target temperature was reached (typically 300–400 °C). Mechanical load was held, while the system cooled to 200 °C to keep a high cooling rate. The temperature was monitored using one K-type thermocouple placed at the outer die ID–inner die OD interface. Density of bulk samples was calculated through geometric means and the Archimedes method.

Structural and microstructural characterization

X-ray diffraction (XRD) (PANalytical Empyrean Diffractometer with Cu Kα X-ray source $\lambda K\alpha_1$ = 1.54056 Å, $\lambda K\alpha_2$ = 1.54440 Å using 0.01313° step size) was used for compositional characterization. XRD peak intensity ratios were used to estimate relative phase composition. The highest intensity peak of a particular phase was divided by the summation of the highest intensity peaks of the detectable phases. Microstructural characterization was done by scanning electron microscopy (SEM) (Philips XL30).

Magnetic measurements

Magnetic measurements were attained using a vibrating-sample magnetometer (VSM) (Lakeshore 7400 Series) at room temperature. Hysteresis loop measurements with maximum field values of 1.6 T were measured in order to obtain magnetization, m [emu] versus applied field, H [Oe]. Magnetization was normalized by mass for powders, yielding σ [emu/g] and by volume for densified samples yielding M [emu/cm^3]. Coercivity, H_c [Oe], remanence magnetization M_r [emu/g] and saturation magnetization M_s [emu/g] was extracted from the σ *vs.* H and M versus H hysteresis curves. The non-saturating slope, due to SFO being ferrimagnetic, was subtracted when calculating M_s. Energy product, $(BH)_{max}$ [MGOe] for powders, was calculated assuming full density of SFO. Actual measured density (Archimedes method) was used to determine $(BH)_{max}$ for the bulk composites. Although no demagnetization factor was used in calculating magnetic induction, magnetic measurements were taken on samples of similar cube geometries to ensure comparability.

First-order reversal curve (FORC) measurements were attained by increasing the magnetic field to 0.6 T then decreasing the field to a reversal field of H_a, then, ramping back up to 0.6 T through magnetic field values of H_b. Step size of 200 Oe was used. Volume-normalized magnetization, M, as a function of H_a and H_b, $M(H_a, H_b)$, was calculated and recorded. The procedure was repeated from 5800 to −6000 Oe to attain a number of first-order reversal curves in 200 Oe intervals. FORC distribution, ρ, is calculated using the relation [22]:

$$\rho(H_a, H_b) = -\frac{\partial^2 M(H_a, H_b)}{\partial H_a \partial H_b} \quad (1)$$

FORCinel software was used to obtain the FORC distribution and plot ρ, as a function of (H_c, H_u) where $H_c = (H_b - H_a)/2$ and $H_u = (H_a + H_b)/2$ [23].

Results and discussion

Soft phase powder

In order to understand the chemical synthesis and reduction behavior of the desired soft magnetic material, the Co-based phase was investigated individually (without the SFO hard phase). There has been previous work on the chemical synthesis of Co–O and Co–O–H [24, 25]. Similar to our previous work with Fe–O [6], we chose to synthesize the Co–O/Co–O–H soft phase precursor through homogeneous precipitation method by decomposition of urea. We select this method because it results in excellent control of grain size and nanoscale phase distribution. $Co(NO_3)_2$ was used as cation source and the NH_4NO_3 which formed as by-product is easily removed during heat treatment.

XRD patterns of as-precipitated powder (without SFO) are shown in Fig. 2a. Broad peaks that can be attributed to the metal hydroxide $Co(OH)_2$ are a present in the as-precipitated powder. In order to obtain the desired metal Co by the conversion of $Co(OH)_2$–Co, the as-precipitated powder was treated in 95% N_2: 5% H_2 gas flow at elevated temperatures.

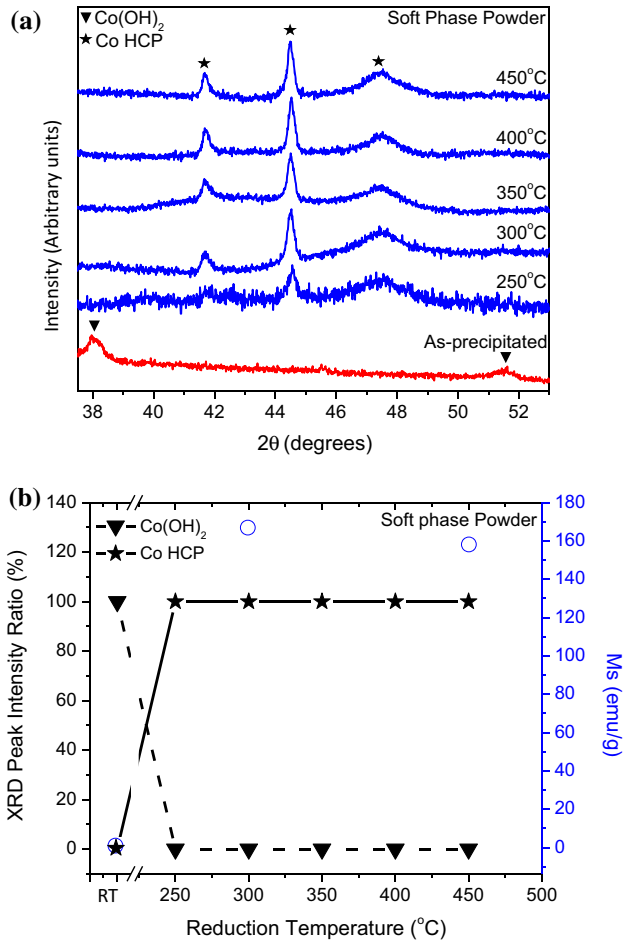

Figure 2 **a** X-ray diffraction patterns for the Co-based soft phase after precipitation as well as at reduction temperatures 300–450 °C. **b** XRD peak intensities ratios of the Co-based soft phase after precipitation as well as at reduction temperatures 300–450 °C. The peak intensity ratio is the ratio of the most intense peak of a particular phase to the sum of the intensities of the most intense peaks of all identifiable phases. The most intense peaks for Co and $Co(OH)_2$ are from the (111) and (011) planes, respectively. The horizontal axis is broken into room temperature results (marked RT) and annealing temperature. Also shown is the saturation magnetization (M_s) of the Co-based soft phase after precipitation as well as at reduction temperatures 300 °C and 450 °C.

Figure 2a shows XRD patterns of the powders reduced at 250 °C–450 °C. The XRD of the powder treated at 250 °C shows that $Co(OH)_2$ has been converted to Co; All present XRD peaks can be attributed to the hexagonal close-packed (HCP) Co phase, which is the expected low-temperature equilibrium structure. As the temperature is raised to 300 °C, the signal-to-background ratio increases, suggesting a higher degree of crystallinity in the powder. Further increases of temperature 350–450 °C does not show significant changes in XRD patterns. The phase evolution of the soft phase is easily appreciated in Fig. 2b, which shows XRD peak intensity ratio versus reduction temperature. By the relatively low temperature of 250 °C, all of the soft phase XRD peaks are those belonging to Co. This is important in regards to magnetic composite formation since a relatively high conversion temperature would make unfavorable reaction between the desired magnetic phases more likely.

The M_s of the soft phase particles post-precipitation as well as at reduction temperatures of 300 °C and 400 °C is also shown in Fig. 2b. The as-precipitated powder (0 °C) has a very low M_s = 0.9 emu/g which is consistent with the XRD results showing that the powder is $Co(OH)_2$. After the reduction at 300 °C, the M_s increases dramatically to 166 emu/g, which is also consistent with XRD results showing the powder is mostly Co (M_s = 193 emu/g for Co [26]). The M_s stays consistent at reduction temperatures 300 °C and 450 °C.

Composite powder

Co-based soft phase precursor was precipitated heterogeneously on the surface of SFO. As mentioned in the experimental Sect. (Nanocomposite powder synthesis), gravimetric analysis was used to find the precipitation yield. The calculated yield of the precipitation process, based on the amount of Co, was different depending on the initial ratio of SFO/Co used. For the SFO/Co mass ratios of 1:1, the yields of Co precipitation were 19.8% meaning 80.2% of initial Co was removed by the decantation. For the 1:2 and 1:4 samples, the yields were 21.8% and 25.4%, respectively (under 1 h precipitation conditions).

As discussed above, the ideal Co layer, L_{Co}, surrounding the SFO phase is ~ 10.5 nm. Using the measured precipitation yield and the measured average size of SFO particles, we can estimate the thickness of the resultant Co layers on the SFO particles. Assuming hexagonal platelet geometry for SFO and perfect (continuous and uniform thickness) coverage on the SFO particles and that all soft phase transforms to Co, the Co layer shells should range from thicknesses of L_{Co} = 4 nm (for 1:1 SFO/Co ratio) to L_{Co} = 20 nm (for 1:4 SFO/Co ratio). Under these assumptions, an initial mass precipitation ratio of SFO/Co at 1:2.23 should yield the ideal

L_{Co} = 10.5 nm thickness. 1:2.23 ratio is very close to the investigated ratio of 1:2.

XRD plots of as-precipitated as well as reduced (250–500 °C) SFO-/Co-based composite using a 1:2 SFO/Co are shown in Fig. 3a. The as-precipitated composite displays peaks belonging to CoO_2 and SFO, with the SFO phase dominating as expected due to the low yield of Co precipitation (21.8%). At the reduction temperature of 250 °C, the composite shows XRD peaks belonging to CoO_2, SFO and Co, indicating that some Co–O has converted to Co. Interestingly, face-centered cubic (FCC) peaks are observed in this composite case, while peaks observed in pure soft phase (Fig. 2) are HCP Co. The Fe–Co phase diagram [27] shows an FCC solid solution at the Co-rich compositions. The FCC peaks are evidence of some reaction between the metal Co and oxide SFO to form an (Co, Fe) FCC solid solution. Increasing reduction temperature causes the peaks of CoO_2 to disappear indicating full conversion to metal. In addition, peaks of (Co, Fe) with a body-centered cubic (BCC) structure appear. Even, higher reduction temperature causes the intensity of SFO peaks to decrease and the intensity of (Co, Fe) peaks to increase; here, the Co is acting as a catalyst, which reduces SFO and reacts with Fe to form Co–Fe.

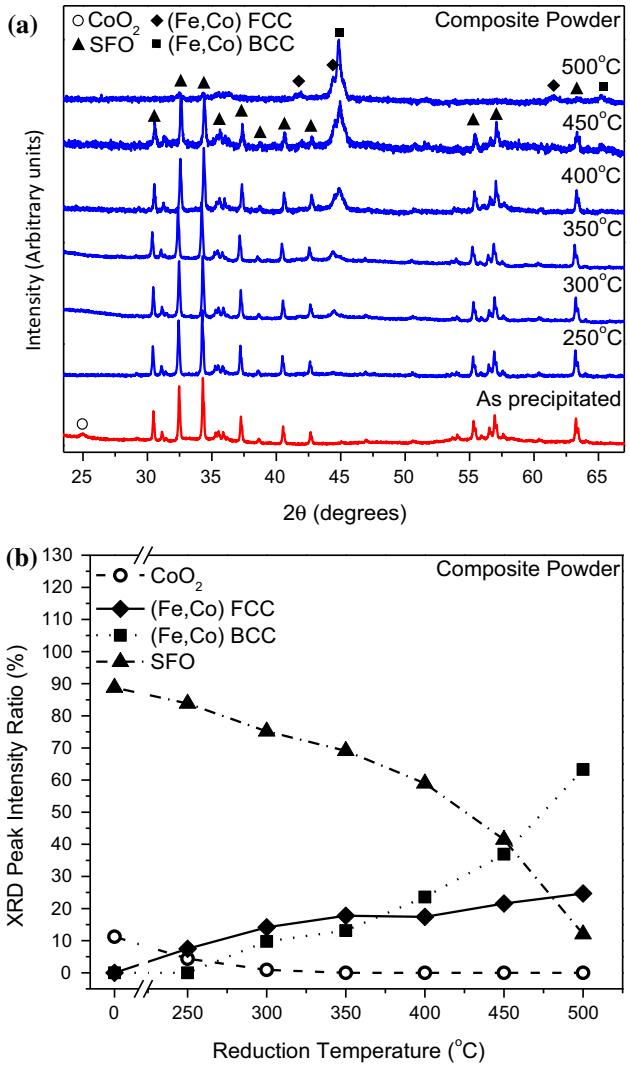

Figure 3 **a** X-ray diffraction patterns for the SFO-/(Co, Fe)-based composite after precipitation procedure as well as at reduction temperatures 250–500 °C. **b** XRD peak intensities ratios of SFO-/(Co, Fe)-based composite after precipitation procedure as well as at reduction temperatures 250–500 °C. The peak intensity ratio is the ratio of the most intense peak of a particular phase to the sum of the intensities of the most intense peaks of all identifiable phases. The most intense peaks for CoO_2, (Co, Fe) FCC, (Co, Fe) BCC and SFO are from the (004), (111), (110) and (107) planes, respectively.

The evolution of the phases, through peak intensities, is more easily appreciated in Fig. 3b. The SFO peak intensity ratio decreases, while those of (Co, Fe) FCC and (Co, Fe) BCC increase with increasing reduction temperature. The increase in metal content is caused by increased reduction in Co precursor and reaction of the Co with Fe in the original SFO phase. This reaction confirms intimate contact between the hard and soft phases as necessary for good magnetic coupling. As the reduction temperature increases further, the peak intensity ratio of (Co, Fe) BCC surpasses that of (Co, Fe) FCC. This suggests the composition evolves to the more Fe-rich BCC solid solution in the two-phase solid solution region of the phase diagram, consistent with higher degree of reaction at higher temperatures. At reduction temperatures above 450 °C (Co, Fe), BCC has the highest intensity ratio. At 450 °C and higher, the ratio of hard phase SFO to soft phase (Co, Fe) is too low to lead to efficient exchange coupling. On the other hand, at reduction temperatures of 300–400 °C, SFO continues to have higher XRD peak intensity ratio than the metal phases, which could lead to a favorable nanostructure for magnetic coupling.

SEM micrographs of the bare SFO (a–c), SFO/(Co–Fe–O) and SFO/(Co, Fe) composites after reduction (d–f) are shown in Fig. 4. The bare SFO powder shows some hexagonal flakes with smooth, featureless surfaces and sharp, faceted edges.

After precipitation and reduction at 400 °C, homogenous coverage of SFO particles is clearly observed at lower magnification in Fig. 4d, e. This

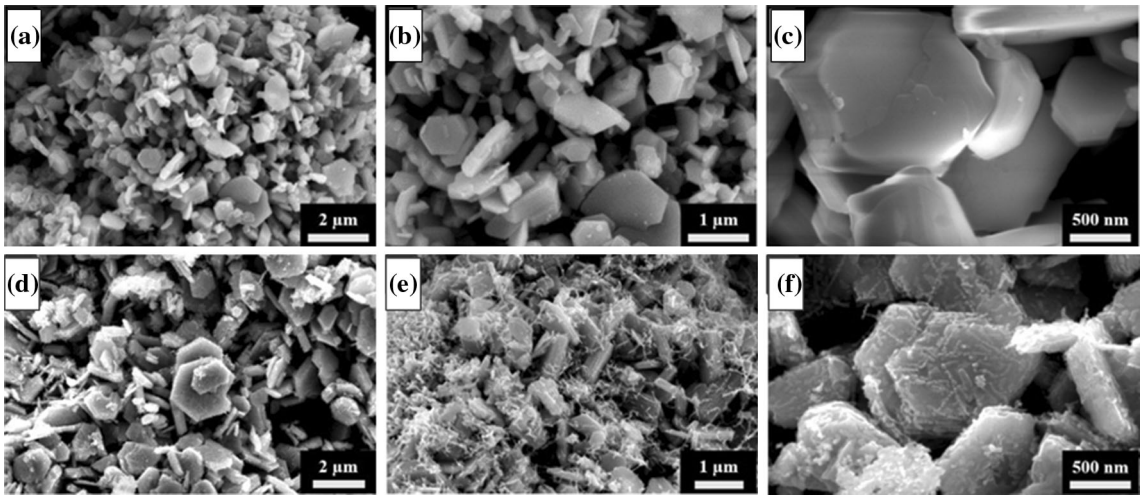

Figure 4 SEM characterization of powders **a**–**c** micrographs of single-phase SFO powder, **d**–**f** SEM micrographs of SFO/(Co, Fe) composite powder after precipitation and reduction at 400 °C.

suggests that the Co precursor precipitate covered the surface of SFO which is energetically favored site for heterogeneous nucleation. The results show that the originally smooth SFO surface was fully covered with granular-shaped particles with dimensions in the tens of nanometers (well presented in dotted circle in Fig. 4f). The underlying SFO still displays faceted edges, suggesting no damage (such as dissolution) to the hard phase as the result of the precipitation procedure as confirmed by XRD. The overall shape of SFO particles is unchanged, suggesting little or no damage to the SFO hard magnetic phase. The calculated thicknesses of soft phase based on yield is in tens of nanometers, if perfect coverage is assumed; this is consistent with visible observations of the SFO/(Co, Fe) composite micrographs.

Hysteresis loops of the SFO/(Co, Fe) powder (1:2 mass ratio) reduced at 350 °C are shown in Fig. 5. For comparison, we also plot results from our previous study on the SFO/Fe_3O_4 system (from REF. [6]) and as-synthesized (bare) SFO. M_s of the SFO/(Co, Fe) composite is higher than that of the SFO/Fe_3O_4 composite. This is consistent with the higher M_s of the (Co, Fe) soft phase compared to Fe_3O_4 soft phase. The higher H_c in the SFO/(Co, Fe) composite compared to SFO/Fe_3O_4 composite is attributed to better coupling and/or less degree of reaction between the hard and soft phases. SFO/Fe_3O_4 composite powder had higher energy product than single-phase SFO, due to exchange coupling between the SFO–Fe_3O_4 [6]. Interestingly, SFO/(Co, Fe) composite has even higher energy product than the SFO/Fe_3O_4 composite, judging by the hysteresis loop in Fig. 5. With higher magnetization at every H in the second quadrant, the energy product $(BH)_{max}$ of the SFO/(Co, Fe) system is clearly higher than that of SFO-/Fe_3O_4-based system. SFO/(Co, Fe) composite powder displays a smooth second-quadrant hysteresis curve (no kink) which is one indicator of exchange coupling.

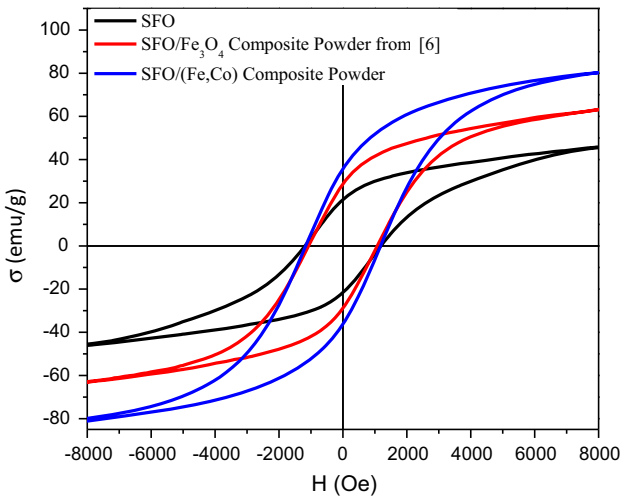

Figure 5 **a** Comparison of hysteresis loop of SFO powder, SFO/Fe_3O_4 (oxide/oxide) composite powder [from ref. 6] and SFO/(Fe, Co) (oxide/metal) composite powder.

Further evidence of coupling in our SFO/(Co, Fe) powder in the FORC diagrams is shown in Fig. 6. Like the SFO/Fe_3O_4 FORC diagram (Fig. 6b), the SFO/(Co, Fe) FORC diagram (Fig. 6c) shows single 'hot spot' suggesting well-coupled hard/soft phases.

In addition, there is a higher spread in H_u for the SFO/(Co, Fe) system compared to the SFO/Fe_3O_4 composite (Fig. 6b) and SFO (Fig. 6a). A larger spread of H_u data is evidence of more particle interactions in the composite material [28]. The magnitude of ρ is highest in the SFO/(Co, Fe) composite, followed by the SFO/Fe_3O_4 composite and lastly single-phase SFO. A higher maximum ρ value (Eq. 1) indicates more ferromagnetic interactions [29, 30]. The location of the maximum ρ value provides further evidence of the nature of magnetic interactions. A hot spot below the H_u=0 axis indicates exchange style interaction [29]. The hot spot peak for the SFO-/Co-based composite is located at $H_u = -224$, Oe further demonstrating effective exchange coupling between SFO and Co.

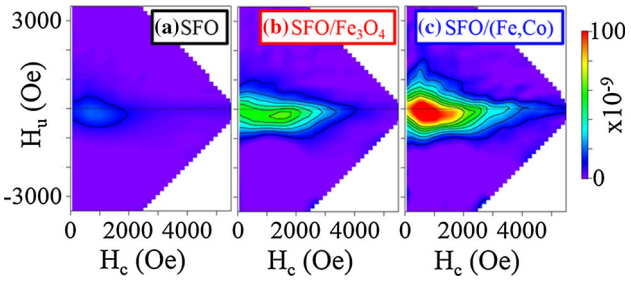

Figure 6 First-order reversal curve (FORC) measurements for **a** single-phase SFO powder, **b** SFO/Fe_3O_4 composite powder (reduced at 400 °C) and **c** SFO/(Co, Fe) composite powder (reduced at 350 °C).

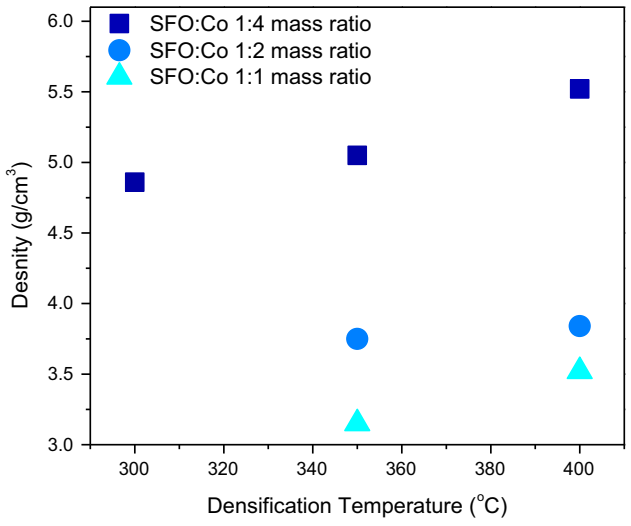

Figure 7 Effect of densification temperature, from 300 to 400 °C, on the density of bulk SFO/(Co, Fe) composite with various starting SFO/Co initial precipitation mass ratios (reduced at 350 °C).

Bulk nanocomposites

High magnetic performance requires a high volume density of magnetic moments in the magnet. We

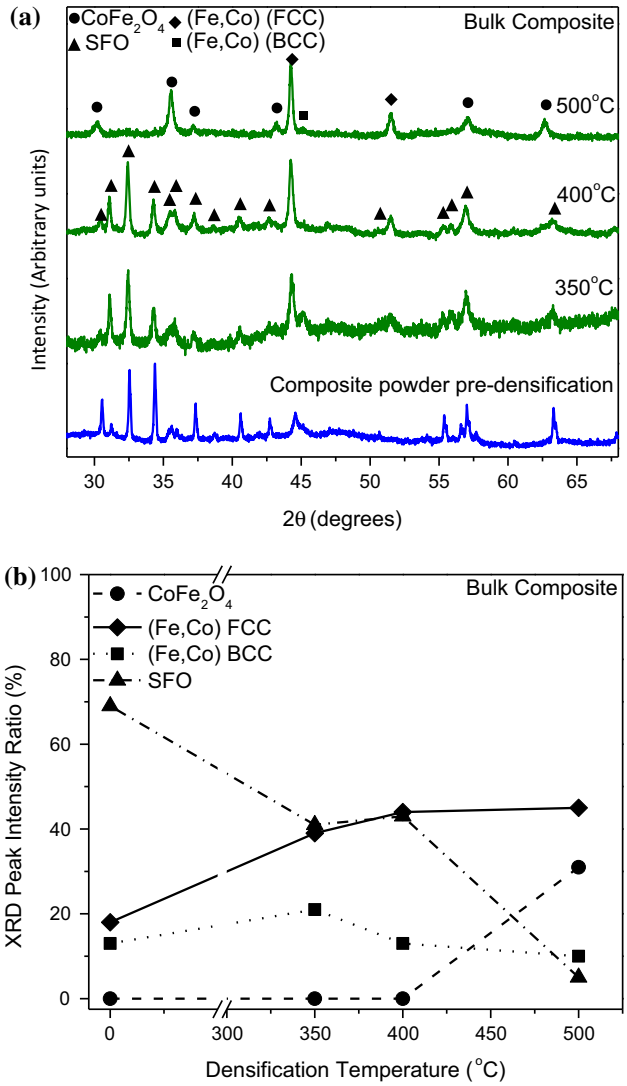

Figure 8 **a** X-ray diffraction patterns for bulk SFO/(Co, Fe) composites densified at 350 °C, 400 °C and 500 °C as well as SFO/(Co, Fe) composite powder (1:2 SFO/Co initial mass precipitation ratio powder reduced at 350 °C). **b** XRD peak intensities ratios of SFO/(Co, Fe) densified composites at varying densification temperatures (0 °C is the composite powder). The peak intensity ratio is the ratio of the most intense peak of a particular phase to the sum of the intensities of the most intense peaks of all identifiable phases. The most intense peaks for $CoFe_2O_4$, (Co, Fe) FCC, (Co, Fe) BCC and SFO are from the (311), (111), (110) and (107) planes, respectively.

therefore densified our composite powders into bulk magnets using CAPAD. The powder results show that powders reduced at intermediate temperatures have the most promising SFO to metal compositions, therefore, we chose powders reduced at 300 and 350 °C for the densification studies. Figure 7 shows the measured bulk density of composites densified from various composite powders (reduced at 350 °C) as a function of densification temperature. As expected, the higher Co content samples have highest overall density since Co is the densest component. In addition, the density of the samples increases with densification temperature for all three compositions.

XRD plots in Fig. 8a and XRD peak intensity ratios in Fig. 8b show phase evolution of the composites densified at various temperatures from starting powder reduced at 350 °C. The ratio of SFO to metal changes after densification showing clear intensity ratio changes in XRD. For example, densifying the oxide/metal composite powder at relatively low densification temperature of 350 °C causes a decrease in SFO and an increase in (Co, Fe) FCC and (Co, Fe) BCC metallic soft phases. This increase in peak ratios can be caused by the increase in crystallinity of metal phase and grain growth. The reaction between Co and SFO is significantly pronounced over 400 °C. The increased temperature and interface area between SFO and metal layers as the densification process progresses accelerate the reaction. At densification temperature of 500 °C, the SFO is almost completely diminished, and the $CoFe_2O_4$ phase appears. It is clear that in order to keep the desired SFO hard phase with proper hard/soft ratio, densification temperature must be kept to low. However, in order to synthesize a composite with relatively high density (as is required for good magnetic performance), a higher densification temperature is preferred. These competing effects between beneficial density and deleterious reaction require the identification of a temperature 'processing window' in order to achieve the desired nanostructure.

Despite the challenge, nanostructural evaluation shows that we were successful in identifying conditions in the processing window. Figure 9 qualitatively shows the effect of SFO/Co initial mass ratio on the composite microstructure. The darker gray regions are SFO, while the brighter regions are metal (Co, Fe) as identified by XRD and confirmed using EDS spot analysis (not shown here). The micrograph of SFO/Co ratio of 1:4 (Fig. 9a, b) leads to well-dispersed soft phase/hard phase without significant agglomeration. Higher magnification images (Fig. 9c,

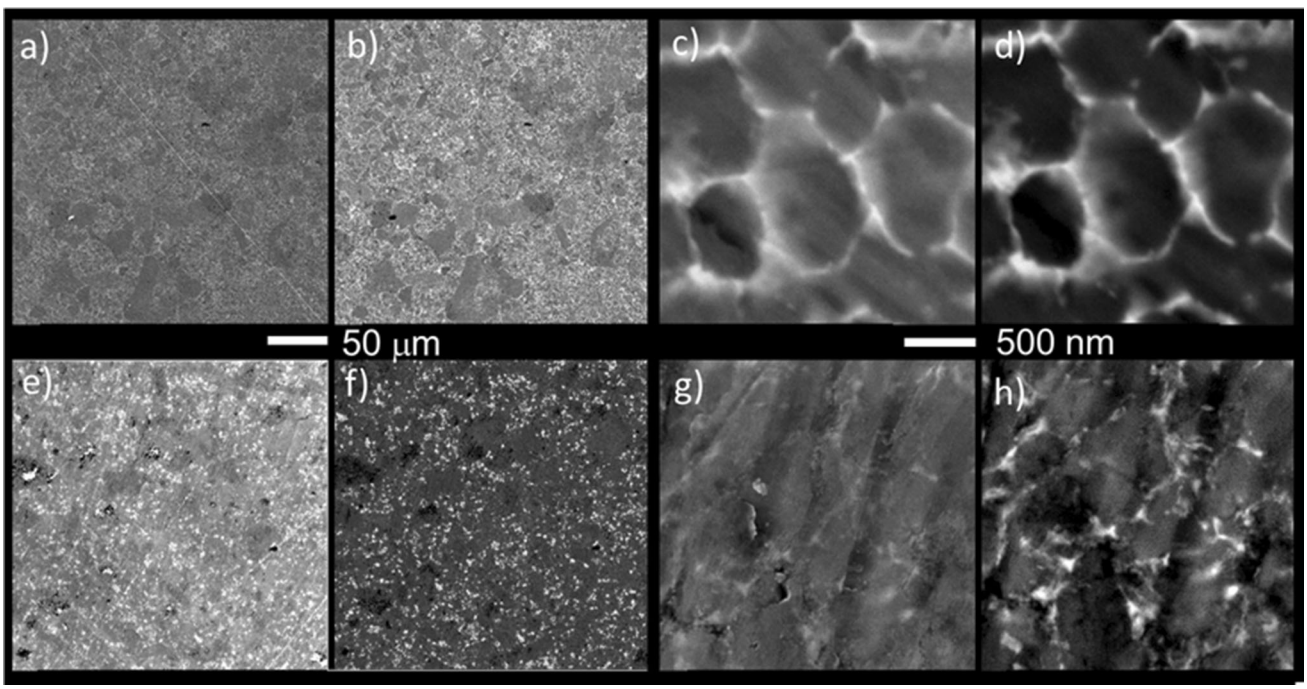

Figure 9 SEM micrographs of bulk SFO/(Co, Fe) composites densified at 400 °C, 505 MPa and no hold time at temperature. Bulk samples were made of powder that has a starting precipitation mass ratio of SFO/Co of **a**–**d** 1:4 and **e**–**h** 1:2.

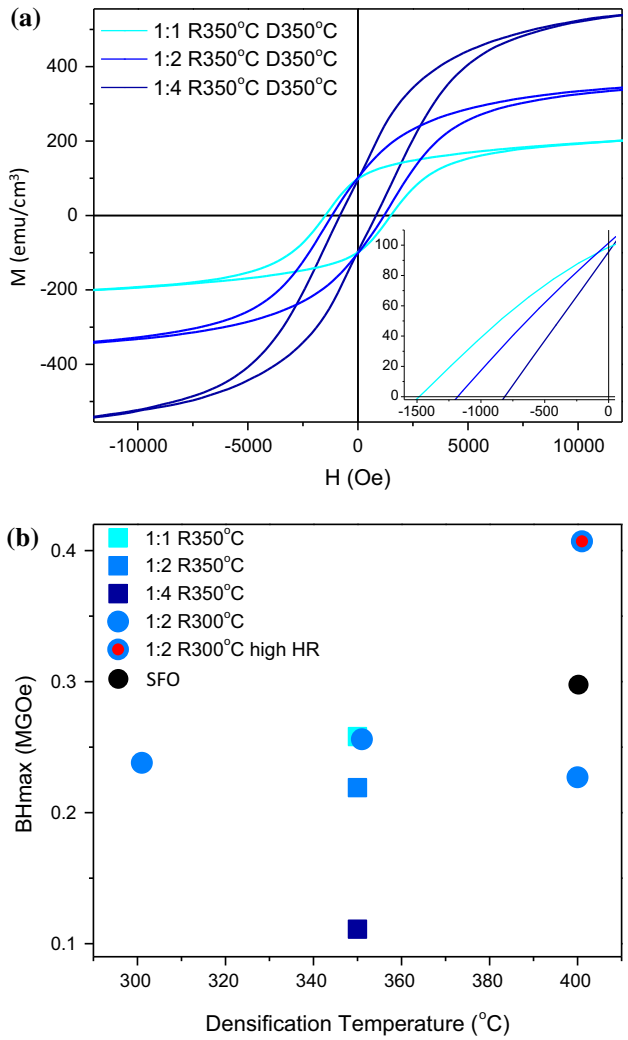

Figure 10 **a** Hysteresis loops of bulk SFO/(Co, Fe) composites processed at densification temperature of 350 °C, SFO/Co initial mass precipitation ratios (1:1, 1:2, 1:4), reduction temperature 350 °C and densification heating rates ~ 90 °C/min. **b** Energy product of bulk SFO/(Co, Fe) composites at various densification temperatures (300–400 °C), SFO/Co initial mass precipitation ratios (1:1, 1:2, 1:4), reduction temperatures (350 °C and 300 °C) and densification heating rates (~ 240 °C/min for high heating rate and ~ 90 °C/min for conventional heating rate.

d) clearly show the (Co, Fe) phase surrounding grains of SFO hard phase, which was our intended well-integrated metal/oxide nanostructure for attaining efficient magnetic coupling. Similarly, the 1:2 SFO/Co composite system (Fig. 9e, f) also reveals well-intermixed SFO/(Co, Fe); the metal layers are thinner which is consistent with the lower Oxide/Metal starting ratio. In addition, there is no clear evidence of porosity in either of these bulk composites.

As mentioned earlier, magnetic performance depends on phase composition, density and interfacial contact area, which as seen from XRD and densification results depend on processing conditions. As an example, the effect of starting mass ratio on magnetic behavior of densified composites is shown in Fig. 10a, which shows magnetic hysteresis of bulk composites densified at 350 °C from powder reduced at 350 °C. It is worth noting that M_s of the densified samples can now be reported in the preferred units of emu/cm^3 instead of emu/g since the density of the samples was measured using Archimedes method. The M_s clearly decreases, while the H_c increases as the metal content decreases. The decrease in H_c is likely caused by increased concentration of soft phase moments which can easily rotate in the applied magnetic field. The inset on figure (magnification of second quadrant) shows that the 1:1 composite has the largest area under the hysteresis curve, implying the highest $(BH)_{max}$ and making it the best PM of this set of samples.

The energy product $(BH)_{max}$ of all of the samples in this study is displayed in Fig. 10b. The $(BH)_{max}$ for single-phase SFO found in this study (0.29 MGOe) is also plotted for comparison. The varying processing temperatures are densification temperatures (300–400 °C), SFO/Co initial mass precipitation ratios (1:1, 1:2, 1:4), reduction temperatures (350 °C and 300 °C) and densification heating rates (~ 240 °C/min and ~ 90 °C/min). Although 1:1 samples showed the highest energy product (at densification temperature of 350 °C), high degree of porosity and lack of improvement in M_r over SFO (not shown here) suggested it is not a good candidate for optimization. 1:2 composite was chosen as it showed the second highest energy product (densified at 350 °C). Optimizing the powder reduction temperature by lowering it from 350 to 300 °C allowed for improvement in energy product of the composite. Sweeping the densification temperature did not improve the energy product. At densification temperature of 300 °C, density was too low. At 400 °C, the higher density did not make up for increase in reaction between hard and soft phases. Ideally, higher density of the higher densification temperature should improve the energy product. By increasing the heating rate during densification, a large improvement in energy product was attained. The increased heating rate allowed for less time spent at elevated temperatures, limiting the detrimental reaction, while the

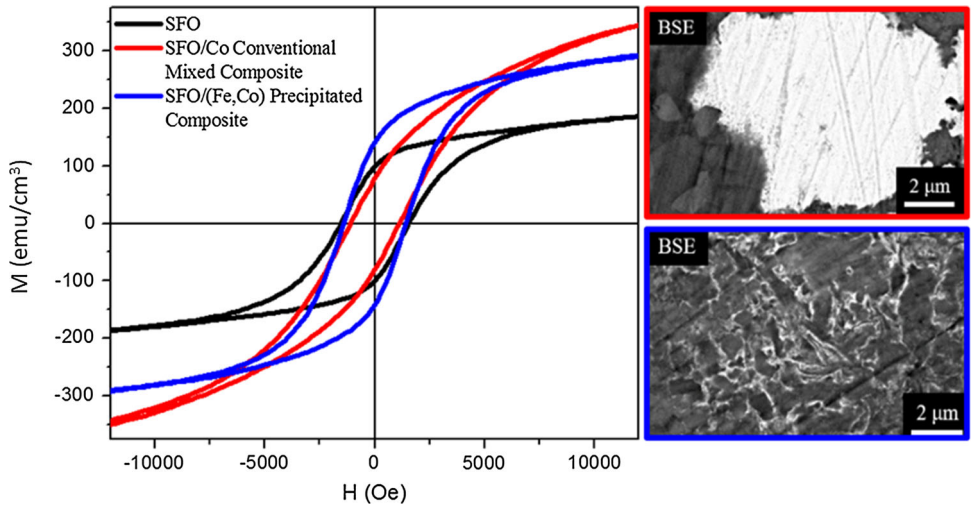

Figure 11 Hysteresis loop of as-densified SFO (at 1000 °C), conventional (hand-mixed) SFO/(Co, Fe) composite (densified at 400 °C, 505 MPa and no hold) and densified SFO/(Fe, Co) composite (synthesized using 1:2 SFO/Co starting ratio powder reduced at 300 °C and densified at 400 °C, 505 MPa and no hold). SEM micrographs of conventional (hand-mixed) SFO/(Fe, Co) composite (top right) and densified SFO/(Co, Fe) composite (bottom right) are also shown.

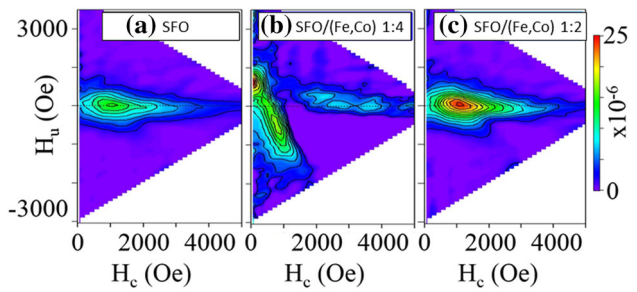

Figure 12 FORC diagrams of bulk SFO and SFO/(Co, Fe) composites densified at the same densification conditions of 400 °C, 505 MPa and no hold time at temperature. **a** SFO, **b** SFO/(Co, Fe) composite with initial precipitation SFO/Co mass ratio of 1:4 and **c** SFO/(Co, Fe) composite with initial precipitation SFO/Co mass ratio of 1:2 (composites synthesized from powder reduced at 300 °C).

higher densification temperature allowed for higher sample density. The 'optimized' sample densified at 400 °C from powder reduced at 300 °C with high HR has a$(BH)_{max}$ of 0.41 MGOe, a 70% improvement in energy product over the single-phase SFO.

In order to highlight the necessity of nanoscale intermixing of the soft/hard magnetic phases that was achieved by precipitation of soft phase onto hard phase (*i.e.*, core–shell powder), we compare with a composite synthesized using conventionally mixed powders followed by CAPAD. Figure 11 shows the hysteresis loops of densified precipitated composite, conventionally mixed composite and single-phase densified SFO for comparison. All samples were densified using the same processing conditions of 400 °C, 505 MPa with no hold at temperature. The conventionally mixed bulk composite has higher M_s, compared to densified SFO, showing the effect of high M_s soft phase. However, the M_r of the composite is lower than that of the single-phase SFO, suggesting decoupled behavior. H_c of the composite is also lower, as expected with a higher volume fraction of decoupled soft phase. These data confirm that conventional processing does not improve magnetic properties (with the exception of M_s) of the composite compared to single-phase SFO.

On the other hand, the SFO/Co composite synthesized using precipitation (*i.e.*, core–shell) method presented here shows significantly improved magnetic properties. The magnetization of the bulk precipitated composite is higher than that of the conventionally mixed SFO/Co and single-phase SFO everywhere in the second quadrant, yielding a higher $(BH)_{max}$. The BSE–SEM micrographs in Fig. 11 reveal the underlying nanostructure that yields the improved properties of the precipitated composite. The precipitated composite displays a much more uniform distribution of soft phase (light region) as needed for coupling (see Fig. 1). By contrast, the soft phase in the conventionally mixed composite is severely agglomerated and therefore not nanoscale. This microstructure cannot lead to efficient coupling between SFO and Co phases since the Co

agglomeration is much larger than the exchange length, L_{ex}. It is possible that a higher degree of mechanical motion/energy can improve mixing, but it would almost certainly damage the SFO particles resulting the reduction in magnetic properties.

In order to confirm that the increased $(BH)_{max}$ of the bulk precipitated composites is due to exchange coupling, we performed FORC analysis. Figure 12 shows FORC diagram for bulk (a) SFO, (b) an SFO/(Co, Fe) composite densified from powders with 1:4 starting precipitation ratio and (c) an SFO/(Co, Fe) composite densified from powders with 1:2 starting precipitation ratio. The single-phase SFO sample (a) shows a single 'hot spot' which is expected for a single component magnet. By contrast, the 1:4 starting precipitation ratio sample (b) shows multiple 'hot spots', indicative of a decoupled multi-component magnet. This can be attributed to the composite having excess (Co–Fe) phase which is not efficiently coupled to the hard phase SFO. Finally, the single hot spot behavior shown in the FORC diagram of the optimized composite resembles the single-phase behavior of bulk SFO, but with higher ferrimagnetic interaction. In essence, the exchange coupling causes the two phases to behave as one exchange couple phase.

Summary

In summary, we introduce a synthesis/processing method for fabricating dense oxide/metal nanocomposites from core–shell powders. We establish a processing window (for both the powder reduction and densification steps) that yields high density composites with minimal interfacial reaction. Through optimization of powder synthesis and fine control of microstructure, a 70% improvement in energy product of bulk, RE free, exchange-coupled nanocomposite is observed, compared to single-phase bulk SFO hard phase.

Acknowledgements

The support of this work from the Office of Naval Research with Dr H. S. Coombe as program manager is most gratefully acknowledged.

References

[1] Hellman F et al (2017) Interface-induced phenomena in magnetism. Rev Mod Phys 89:025006

[2] Miyazaki T, Tezuka N (1995) Giant magnetic tunneling effect in Fe/Al_2O_3/Fe junction. J Magn Magn Mater 139:L231–L234

[3] Tang C, Sellappan P, Liu Y, Xu Y, Garay JE, Shi J (2016) Anomalous hall hysteresis in Tm3Fe5O12/Pt with strain-induced perpendicular magnetic anisotropy. Phys Rev B Rapid Commun 94:140403(R)

[4] Leite GCP, Chagas EF, Pereira R, Prado RJ, Terezo AJ, Alzamora M, Baggio-Saitovitch E (2012) Exchange coupling behavior in bimagnetic $CoFe_2O_4$/$CoFe_2$ nanocomposite. J Magn Magn Mater 324:2711–2716

[5] Zeng H, Li J, Liu JP, Wang ZL, Sun S (2002) Exchange-coupled nanocomposite magnets by nanoparticle by self-assembly. Nature 420:395–398

[6] Volodchenkov AD, Kodera Y, Garay JE (2016) Synthesis of strontium ferrite/iron oxide exchange coupled nano-powders with improved energy product for rare earth free permanent magnet applications. J Mater Chem C 4:5593–5601

[7] Zhang Y, Yan B, Ou-Yang J, Zhu B, Chen S, Yang X, Liu Y, Xiong R (2015) Magnetic properties of core/shell-structured CoFe2/CoFe2O4 composite nano-powders synthesized via oxidation reaction. Ceram Int 41:11836–11843

[8] Fullerton Eric E, Jiang JS, Grimsditch M, Sowers CH, Bader SD (1998) Exchange-spring behavior in epitaxial hard/soft magnetic bilayers. Phys Rev B 58:12193

[9] Garay JE (2010) Current activated pressure assisted densification of materials. Annu Rev Mater Res 40:445–468

[10] Morales JR, Tanju S, Beyermann WP, Garay JE (2010) Exchange bias in large three dimensional iron oxide nanocomposites. Appl Phys Lett 96:013102

[11] Zhang Y, Xiong R, Yang Z, Yu W, Zhu B, Chen S, Yang X (2013) Enhancement of interparticle exchange coupling in $cofe_2o_4$/$cofe_2$ composite nanoceramics via spark plasma sintering technology. J Am Ceram Soc 96(12):3798–3804

[12] Nawathey-Dikshit R, Shinde SR, Ogale SB, Kulkarni SD, Sainkar SR, Date SK (1996) Synthesis of single domain strontium ferrite powder by pulsed laser ablation. Appl Phys Lett 68(24):3491

[13] Liu Z, Davies H (2009) J Phys D: Appl Phys, vol. 42

[14] Shinde S R, Lofland S E, Ganpule C S, Ogale S B, Bhagat S M, Venkatesan T, and Ramesh R J (1999) Appl Phys 85(10): 7459

[15] Pullar RC (2012) Prog Mater Sci 57(7):1191–1334

[16] Willard HH, Tang NK (1937) A study of the precipitation of aluminum basic sulfate by urea. J Am Chem Soc 1937(59):1190–1196

[17] Djuričić B, Pickering S, McGarry D, Glaude P, Tambuyser P, Schuster K (1995) The properties of zirconia powders produced by homogeneous precipitation. Ceram Int 21(3):195–206

[18] Unuma H, Kato S, Ota T, Takahashi M (1998) Homogeneous precipitation of alumina precursors via enzymatic decomposition of urea. Adv Powder Technol 9(2):181–190

[19] Matijevic E (1993) Preparation and properties of uniform size colloids. Chem Mater 5(4):412–426

[20] Parida K, Das J (1996) Studies on ferric oxide hydroxides: II. Structural properties of goethite samples (α-FeOOH) prepared by homogeneous precipitation from $Fe(NO_3)_3$ solution in the presence of sulfate ions. J Colloid Interface Sci 178(2):586–593

[21] Anselmi-Tamburini U, Garay JE, Munir ZA (2006) Fast low-temperature consolidation of nanometric ceramic materials. Scr Mater 54:823–828

[22] Pike CR (2003) First-order reversal-curve diagrams and reversible magnetization. Phys Rev B 68(10):104424

[23] Harrison R J and Feinberg J M (2008) "FORCinel: An improved algorithm for calculating first-order reversal curve distributions using locally weighted regression smoothing," Geochemistry, Geophys. Geosystems 9(5)

[24] Jiang Y, Wu Y, Xie B, Xie Y, Qian Y (2002) Moderate temperature synthesis of nanocrystalline Co 3 O 4 via gel hydrothermal oxidation. Mater Chem Phys 74:234–237

[25] Yang H, Hu Y, Zhang X, Qiu G (2004) Mechanochemical synthesis of cobalt oxide nanoparticles. Mater Lett 58(3–4):387–389

[26] Fullerton EE, Jiang J, Bader S (1999) Hard/soft magnetic heterostructures: model exchange-spring magnets. J Magn Magn Mater 200(1–3):392–404

[27] Nishizawa T, Ishida K (1984) The Co–Fe (cobalt–iron) system. Bull Alloy Phase Diagr 5(3):250–259

[28] Pike CR, Roberts AP, Verosub KL (1999) Characterizing interactions in fine magnetic particle systems using first order reversal curves. J Appl Phys 85(9):6660

[29] Roy D, Anil Kumar PS (2015) Exchange spring behaviour in SrFe12O19–$CoFe_2O_4$ nanocomposites. AIP Adv 5(7):077137

[30] Mayergoyz ID (2003) Mathematical models of hysteresis and their applications. Second Elsevier, New York

[31] Volodchenkov AD, Ramirez S, Samnakay R, Salgado R, Kodera Y, Balandin AA, Garay JE (2017) Magnetic and thermal transport properties of SrFe12O19 permanent magnets with anisotropic grain structure. Mater Des 125(5):62–68

[32] Chan KT, Morales JR, Kodera Y, Garay JE (2017) A processing route for bulk, high coercivity, rare-earth free, nanocomposite magnets based on metastable iron oxide. J Mater Chem C 5:7911